LETTERS IN BIOMATHEMATICS
An International Journal

RESEARCH ARTICLE

OPEN ACCESS

Empirical modelling for dry sliding wear and friction of sand-cast leaded tin bronze (LTB): Effects of load, speed and hardness

Ram Dhani Chauhan[a,*], Prem Kumar Bharti[a]

[a] Department of Mechanical Engineering, Integral University, Lucknow, India
* Corresponding author. E-mail address: rdc9100@gmail.com (R.D. Chauhan).

ABSTRACT

Leaded tin bronze (LTB) is the standard material for submersible pump bushes, yet few tools exist for predicting its wear. Seven sand-cast LTB alloys (7–14 wt% Sn, 10–16 wt% Pb; 57–112 BHN) were tested against EN31 steel on a pin-on-disc tribometer, and empirical wear and friction models were developed and independently checked. For the LTB 5-grade alloy Cu–10Sn–10Pb–2Ni–1Zn (88 BHN) at 10–50 N and 500–1500 rpm, mass loss rose tenfold (0.026–0.265 g), whereas the specific wear rate (SWR) stayed within 2.51–4.30 × 10^{-6} g/N·m, consistent with Archard-type scaling. The coefficient of friction (COF) varied non-monotonically between 0.208 and 0.430. A power-law load–speed model captured mass loss with R^2 = 0.950 (MAPE = 10.7%), and a linear interaction model described COF with R^2 = 0.735. Wear resistance did not scale with hardness: the hardest alloy (112 BHN) lost the most mass (0.690 g) due to formation of intermetallic compound of delta phase which is brittle in nature.. Domestic-water lubrication (50 N, 1500 rpm, 60 min) reduced the SWR from (2.816 ± 0.049) × 10^{-6} to (2.46 ± 0.34) × 10^{-7} g/N·m and the COF from 0.430 to 0.177 ± 0.003, i.e. by 91% and 59%. The dry lubrication generalized LTB mass loss model overpredicted the water-lubricated SWR about elevenfold, which a water-lubrication factor of 0.091 corrects. For a 12.5 hp WPIL submersible pump at its duty point, the water-lubricated SWR gives a conservative bush life of about 603–3928 h.

ARTICLE HISTORY
Received October 15, 2026
Accepted November 19, 2026

KEYWORDS
Leaded tin bronze; Dry sliding wear; Water lubrication; Coefficient of friction; Empirical model; Bush life

1. Introduction

Groundwater pumping is one of the largest consumers of electrical energy in India. The sixth minor irrigation census recorded about 23.1 million minor irrigation schemes, of which about 21.9 million rely on groundwater [1], and a large proportion of these are driven by submersible pumps. In such pumps, the shaft rotates within bush bearings, where friction and wear dissipate energy and ultimately govern service life. Even modest improvements in bush material can therefore translate into substantial energy savings and lower maintenance costs.

Leaded tin bronze (LTB) is the established bush material for this application. The Indian standard IS 318:1981 specifies six grades, LTB 1 to LTB 6 [2]. Pump manufacturers typically employ LTB 3 or LTB 4, which contain 6–8 wt% Sn, whereas grade LTB 5 contains 9–11 wt% Sn and 8.5–11 wt% Pb, with up to 2 wt% Ni and 1 wt% Zn [2]. In earlier work, the authors reviewed the tribology of bronze alloys [3] and experimentally compared sand-cast LTB compositions [4]. That work identified about 9–10 wt% Sn and 10–11 wt% Pb as an optimal range for bushes and proposed a '9-10-11' rule of thumb for the Sn and Pb contents of LTB, with 2 wt% Ni and 1 wt% Zn held constant.

The effectiveness of LTB as a bearing alloy stems from its two-phase microstructure. The Cu–Sn matrix supports the load, while lead, being virtually insoluble in copper, segregates as discrete soft globules, predominantly at the grain boundaries. During sliding, these globules smear across the contact and function as an in situ solid lubricant [3,5,6]. Tin strengthens the matrix, and hardness increases with tin content in cast Cu–Ni–Sn alloys [7,8]; nickel enhances corrosion resistance, and zinc promotes deoxidation and casting soundness. More broadly, bronzes combine good castability, corrosion resistance and thermal conductivity, with properties governed by composition and processing route [9–13].

Processing route exerts an equally strong influence. In cast alloys, faster cooling refines the dendrite arm spacing and raises strength [14,15], and a similar trend in hardness has been reported for an 80Cu–20Sn bronze [16]. Gupta et al. [17] showed that multidirectional forging of a high-leaded tin bronze increased its hardness from 63 to 146 HV and reduced its wear rate, an effect of grain refinement well documented in other alloy systems [18].

The influence of load, speed and microstructure on the wear of bronzes has been examined in several studies. Prasad [5] demonstrated that the sliding wear of bronzes is governed by composition, microstructure and test conditions, while Pathak and Tiwari [6] reported that lead in copper–lead bearing alloys forms a lubricating film on the sliding surface. The wear of spinodal Cu–15Ni–8Sn bronze has likewise been linked to its microstructure and to the evolution of the surface layer during sliding [19,20]. Such results are commonly rationalised by Archard-type reasoning, in which wear volume increases with load and sliding distance and decreases with hardness [21]. LTB bearing alloys of differing composition, however,

can deviate markedly from this simple rule, because transfer layers, oxidation, brittle delta-phase formation and wear debris continuously modify the contact during sliding.

Growing restrictions on lead, owing to its toxicity, have prompted interest in graphite as an alternative solid lubricant in copper alloys. Copper-coated graphite yielded lower wear and friction than uncoated graphite in copper–graphite composites [22], and microwave-sintered copper–nanographite composites exhibited similar benefits [23]. In copper–graphite composites, the coefficient of friction (COF) decreased as the graphite content approached 3–4 wt%, albeit at the expense of hardness [24]. Tin bronze containing about 2.7 wt% nickel-coated graphite outperformed CuSn10Pb10 in both friction and wear in bronze–steel bimetal bearings [25,26]. The present paper is confined to lead-containing alloys; graphite-modified LTB is outside its scope.

Although these studies establish qualitative trends, they offer few simple equations with which a designer can estimate the wear and friction of sand-cast LTB at a given load and speed. Moreover, the extent to which hardness alone accounts for differences between LTB compositions remains unclear, and laboratory wear data are seldom translated into bush-life predictions.

To address these gaps, this study aimed: (i) to quantify the dry sliding mass loss and COF of sand-cast LTB at three loads and three speeds; (ii) to elucidate the interaction between load and speed; (iii) to develop simple empirical models for the mass loss and COF of the Cu–10Sn–10Pb–2Ni–1Zn alloy, which corresponds to grade LTB 5; (iv) to evaluate broader models incorporating hardness and COF across several LTB compositions; (v) to measure the wear and friction of this alloy under water lubrication and use these data as an independent check of the dry models; and (vi) to demonstrate how the water-lubricated wear rate can be used for a first estimate of bush life.

2. Materials and methods

2.1. Alloy preparation

Seven LTB compositions were prepared by sand casting (Table 1). For each alloy, a 1 kg charge was melted in a 2 kg graphite crucible in a pit furnace under open atmosphere (Fig. 1) and heated to about 1200 °C, as measured with a handheld infrared thermometer. Because zinc has the lowest boiling point of the alloying elements, it was added last, once the melt had reached about 1200 °C. The melt was stirred for 30–60 s and poured into a green sand mould consisting of 87% silica sand, 8% clay, 1% additives and 4% moisture, and the castings were cooled in air for 24 h before machining. Because the alloying elements differ widely in density, some non-uniformity was observed in the castings.



Fig. 1. Melting of the LTB charge in the pit furnace.

Two types of specimen were machined from each casting (Fig. 2): 25 mm × 25 mm × 25 mm blocks for chemical analysis, hardness testing and optical microscopy, and pins of 8 mm diameter and 25 mm length for the wear tests.

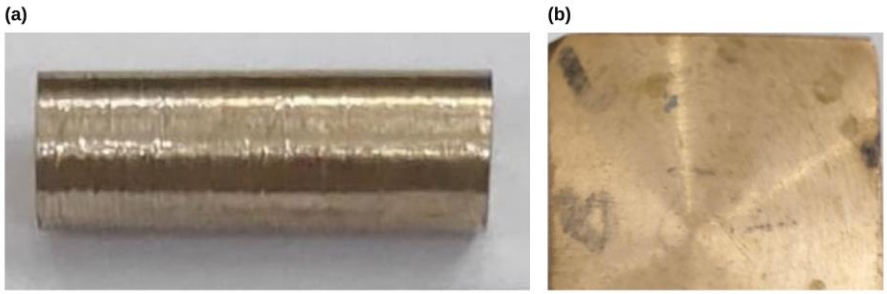

Fig. 2. Machined specimens: (a) wear pin, 8 mm diameter and 25 mm long; (b) 25 mm block for chemical analysis and hardness testing.

2.2. Composition and hardness

Chemical composition was determined by spark optical emission spectroscopy (Arun Technology, PolySpek-F). Microstructure was examined with an optical microscope (Carl Zeiss) following ASM Handbook, Vol. 9 (2004). Brinell hardness was measured with a 5 mm tungsten carbide ball under a load of 750 kgf in accordance with IS 1500 (Part 1):2019, and three readings were averaged for each alloy. Table 1 gives the composition and hardness of the seven alloys. The composition, hardness and screening results of alloys A–G (Table 1) were first reported in our earlier study [27] and are repeated here so that the models can be traced to their source data.

Table 1. Composition (wt%) and Brinell hardness of the cast LTB alloys, with mass loss and COF in the screening test (50 N, 1500 rpm, 10 min).

Sample	Sn	Pb	Zn	Ni	Cu	Hardness (BHN)	Mass loss (g)	COF
A	7	10	0.75	2.0	80.25	69	0.409	0.459
B	9	10	1.00	2.0	78.00	85	0.027	0.560
C	9	16	1.00	2.0	72.00	57	0.341	0.202
D	10	10	1.00	2.0	77.00	88	0.265	0.430
E	10	11	0.75	2.0	76.25	82	0.260	0.343
F	12	12	1.00	3.0	72.00	78	0.110	0.468
G	14	12	1.00	3.0	70.00	112	0.690	0.175

2.3. Wear tests

Wear and friction were measured on a pin-on-disc tribometer. The disc was EN31 steel with a hardness of about 62 HRC and a surface roughness of 0.5–1.5 µm. The pin slid on a track of 20 mm radius, and each test lasted 10 min. Mass loss was determined by weighing the pin before and after each test, and the COF was recorded by the tribometer. The dry tests were run without lubricant.

All seven alloys were first compared in a screening test at 50 N and 1500 rpm (Table 1). Sample D (Cu–10Sn–10Pb–2Ni–1Zn, 88 BHN) was then tested in a full 3 × 3 Taguchi design with loads of 10, 30 and 50 N and speeds of 500, 1000 and 1500 rpm. These loads correspond to nominal contact pressures of 0.20, 0.60 and 0.99 MPa on the 8 mm pin, and the speeds to sliding velocities of 1.05, 2.09 and 3.14 m/s. Samples B, E, F and G were also tested at 10 N and 500 rpm and at 30 N and 1000 rpm.

Because the dry test time was fixed at 10 min, the sliding distance s increased with speed: 628, 1257 and 1885 m at 500, 1000 and 1500 rpm, respectively. To remove the effect of distance, a mass-based specific wear rate was calculated as $k = \Delta m/(L\ s)$, where Δm is the mass loss (g), L is the normal load (N) and s is the sliding distance (m). Each dry test was repeated three times, and mean values are reported. At 50 N and 1500 rpm, the three dry repeats on sample D lost 0.268, 0.260 and 0.268 g and gave a specific wear rate of $(2.816 \pm 0.049) \times 10^{-6}$ g/N·m, and four COF readings (0.445, 0.458, 0.389 and 0.430) gave a mean COF of 0.430 ± 0.030.

Water-lubricated tests were run on sample D at 50 N and 1500 rpm on the same 20 mm track for 60 min (sliding distance 11,310 m), with domestic water supplied to the contact by the lubrication unit of the tribometer (set-up shown in Section 3.8). The test was repeated three times, and the mass loss, specific wear rate and COF are reported as mean ± standard deviation, with 95% confidence intervals (CI) based on the t-distribution.

2.4. Empirical modelling and error measures

The mass loss of sample D was fitted with a power law in load and speed multiplied by a load–speed term, and the COF with a linear model that includes a load × speed product. Broader models that include hardness and COF were then fitted to five alloys. Model quality was assessed by the coefficient of determination (R^2), root-mean-square error (RMSE), mean absolute error (MAE) and mean absolute percentage error (MAPE). All statistics reported here were calculated from the equations and data given in the tables. Finally, the dry models were checked against the water-

lubricated results of sample D, which were not used in any fit. The generalised models were also compared with three further alloys tested in dry sliding at 20 N and 2000 rpm for 8 min (Section 3.7). Two results of Table 4 (samples G and F at 30 N and 1000 rpm), for which the prediction differed from the measurement by more than a factor of 10, were treated as outliers and excluded from Table 4, Fig. 8 and the statistics. Two further alloys (LTB1 and LTB2) were excluded because their Pb contents (3 and 5 wt%) lie below the 10–16 wt% of the fitted alloys. The constants of Eqs. (4)–(6) were derived before these exclusions, using all 15 results, and were not refitted.

3. Results and discussion

3.1. Hardness of the alloys

Hardness ranged from 57 to 112 BHN (Table 1). The hardest alloy, sample G, has the highest tin content (14 wt%), whereas the softest, sample C, has the highest lead content (16 wt%), consistent with solid-solution and intermetallic strengthening by tin and softening by a larger fraction of the lead phase. The trend is not strictly monotonic: sample F (12 wt% Sn, 12 wt% Pb, 78 BHN) is softer than sample D (10 wt% Sn, 10 wt% Pb, 88 BHN), underlining the competing role of lead content.

A composition-based hardness relation developed earlier by the authors is

$$\mathrm{BHN} = 28 + 0.37\mathrm{Cu} + 4.52\mathrm{Sn} + 0.30\mathrm{Ni} - 1.82\mathrm{Pb} - 0.10\mathrm{Zn} \quad (1)$$

where the element symbols denote contents in wt%. The relation was reported with $R^2 = 0.737$ and RMSE = 6.31 BHN within the composition limits of 4.5–15 wt% Sn, 1–20 wt% Pb, 0–4.5 wt% Ni and 0–4.5 wt% Zn. For the seven alloys in Table 1, it gives $R^2 = 0.72$ and RMSE = 8.4 BHN, with the largest error for sample G (predicted 96 BHN, measured 112 BHN). Because the five contents sum to 100 wt%, the coefficients are not independent and should not be interpreted as the separate effect of each element.

Hardness is relevant to wear because a harder matrix resists ploughing and plastic deformation, whereas a sufficient fraction of soft phase is required to sustain a lubricating film. A monotonic decrease in wear with increasing hardness is therefore not expected across all LTB compositions, possibly because brittle delta phase forms at Sn contents above about 10%, a point revisited in Section 3.7.

3.2. Effect of load on mass loss

Table 2. Dry sliding results for sample D (Cu–10Sn–10Pb–2Ni–1Zn, 88 BHN) against EN31 steel; test time 10 min, track radius 20 mm.

Load (N)	Speed (rpm)	Sliding distance (m)	Mass loss (g)	Specific wear rate (10^{-6} g/N·m)	COF
10	500	628	0.026	4.14	0.258
10	1000	1257	0.054	4.30	0.287
10	1500	1885	0.051	2.71	0.311
30	500	628	0.064	3.40	0.235
30	1000	1257	0.130	3.45	0.311
30	1500	1885	0.177	3.13	0.398
50	500	628	0.102	3.25	0.233
50	1000	1257	0.158	2.51	0.208
50	1500	1885	0.265	2.82	0.430

Table 2 and Fig. 3 summarise the results for sample D. Mass loss increased with load at every speed (Fig. 3a): at 500 rpm, it rose from 0.026 g at 10 N to 0.064 g at 30 N and 0.102 g at 50 N, and the corresponding values were 0.054, 0.130 and 0.158 g at 1000 rpm and 0.051, 0.177 and 0.265 g at 1500 rpm. The progressive divergence of the curves with increasing load reveals that the load effect intensifies at higher speed.

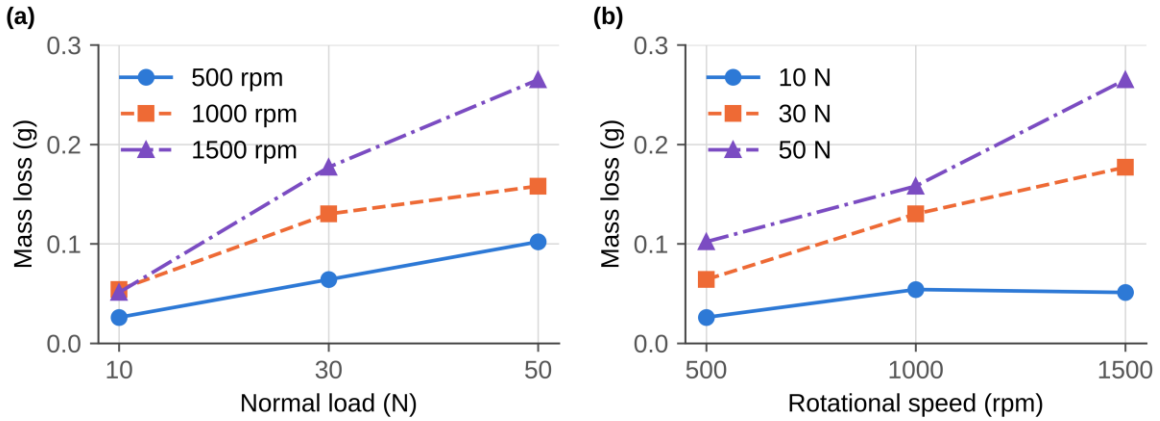

Fig. 3. Mass loss of sample D in a 10 min test: (a) against normal load at three speeds; (b) against rotational speed at three loads.

Higher loads enlarge the real contact area and intensify asperity interactions, so that more material is plastically deformed and removed, in agreement with the observed trends. Averaged over the three speeds, the mass loss was 0.044, 0.124 and 0.175 g at 10, 30 and 50 N, whereas averaged over the three loads it was 0.064, 0.114 and 0.164 g at 500, 1000 and 1500 rpm. Load was therefore the slightly more influential factor over the tested ranges. Both effects far exceed the repeatability of the test: at 50 N and 1500 rpm, the three dry repeats varied by only ±0.049 × 10^{-6} g/N·m in specific wear rate and the four COF readings by only ±0.030, whereas the load effect was about 4.0-fold from 10 to 50 N and the speed effect about 2.6-fold from 500 to 1500 rpm.

3.3. Effect of speed and sliding distance

Mass loss likewise increased with speed, and more steeply at higher load (Fig. 3b). From 500 to 1500 rpm, it rose from 0.026 to 0.051 g at 10 N, from 0.064 to 0.177 g at 30 N and from 0.102 to 0.265 g at 50 N. At 10 N, the value at 1500 rpm (0.051 g) was marginally below that at 1000 rpm (0.054 g); this difference of 0.003 g lies within the probable test error and is not interpreted further.

Part of the apparent speed effect is an artefact of the test design. Because all tests lasted 10 min, a test at 1500 rpm covered three times the sliding distance of one at 500 rpm. Normalising by load and distance removes this effect: the specific wear rate in Table 2 lies between 2.51 × 10^{-6} and 4.30 × 10^{-6} g/N·m, with a mean of 3.30 × 10^{-6} g/N·m, and shows no upward trend with speed. Within this range, mass loss is thus approximately proportional to the product of load and sliding distance, as predicted by an Archard-type relation [21]. The load–speed term in the model of Section 3.4 essentially captures this product and should not be construed as evidence that higher sliding velocity inflicts greater damage per metre of sliding; tests at equal sliding distance are needed to resolve this question.

A lead-rich transfer film is frequently invoked to explain the wear of leaded bronzes [5,6]. Such a film may develop under moderate conditions and break down when load, speed and frictional heating act together. This mechanism offers a plausible explanation of the present trends, and the EDS spectra of the worn surface show lead-rich patches (Section 3.5).

3.4. Mass-loss model for sample D

The nine results in Table 2 were fitted with

$$\Delta m = 9.41 \times 10^{-4}\, L^{0.546}\, N^{0.336} \left[1 + 0.695 \left(\frac{L}{30}\right)\left(\frac{N}{1000}\right)\right] \qquad (2)$$

where Δm is the mass loss in a 10 min test (g), L is the normal load (N) and N is the rotational speed (rpm). Both exponents are positive, and the bracketed term increases the prediction when load and speed are both high.

Table 3. Measured and predicted mass loss and COF for sample D.

Load (N)	Speed (rpm)	Mass loss, measured (g)	Mass loss, Eq. (2) (g)	COF, measured	COF, Eq. (3)
10	500	0.026	0.030	0.258	0.261
10	1000	0.054	0.042	0.287	0.294
10	1500	0.051	0.052	0.311	0.327
30	500	0.064	0.066	0.235	0.228
30	1000	0.130	0.104	0.311	0.297
30	1500	0.177	0.144	0.398	0.366
50	500	0.102	0.102	0.233	0.194
50	1000	0.158	0.175	0.208	0.299
50	1500	0.265	0.255	0.430	0.404

Table 3 and Fig. 4 compare the model with the measurements. The fit gives R^2 = 0.950, RMSE = 0.0162 g, MAE = 0.0118 g and MAPE = 10.7%. A straight line through the predicted and measured values has a slope of 0.935 and an intercept close to zero. The largest errors occur at 30 N, where the model predicts 0.104 g against a measured 0.130 g at 1000 rpm and 0.144 g against 0.177 g at 1500 rpm.

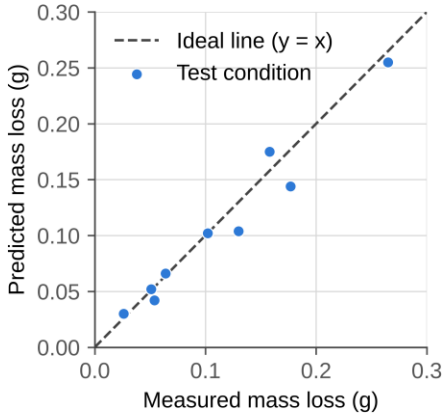

Fig. 4. Measured and predicted mass loss for sample D, Eq. (2).

Two limitations apply. First, the model has four fitted constants and only nine data points, so the statistics above describe how well the equation fits these nine tests; the water-lubricated tests in Section 3.8 provide the only independent check. Second, Eq. (2) was fitted to 10 min tests on a 20 mm track; for another test duration t (min), the mass loss may be estimated by multiplying by t/10, assuming that the wear rate stays constant with time.

3.5. Friction response

In contrast to mass loss, the COF of sample D (Fig. 5) did not vary monotonically with load or speed. At 1500 rpm, it increased with load from 0.311 at 10 N to 0.398 at 30 N and 0.430 at 50 N, whereas at 500 rpm it decreased slightly from 0.258 to 0.235 and 0.233. At 1000 rpm, it rose from 0.287 to 0.311 at 30 N before falling to 0.208 at 50 N. Across the nine tests, the COF spanned 0.208–0.430, with a mean of 0.297.

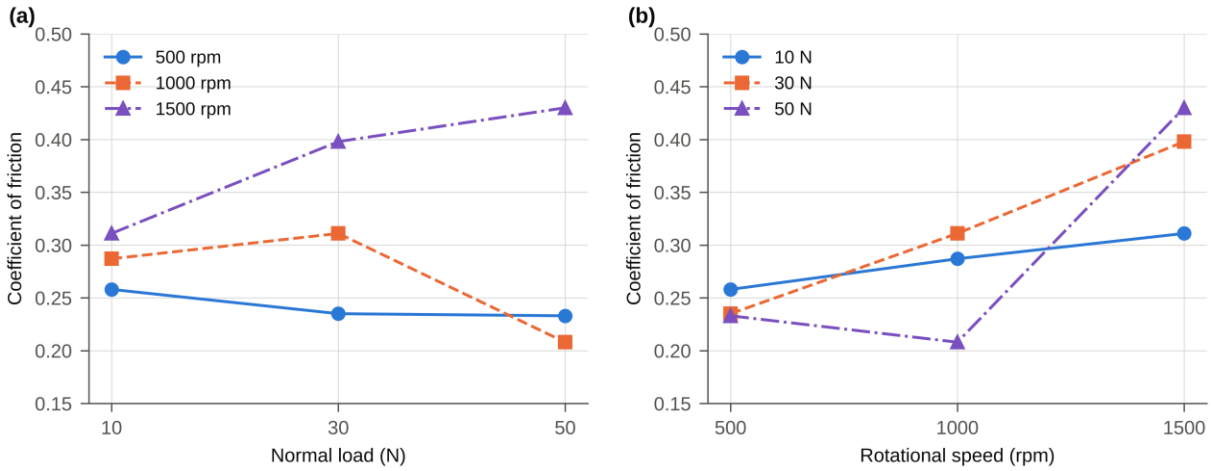

Fig. 5. Coefficient of friction of sample D: (a) against normal load at three speeds; (b) against rotational speed at three loads.

At 50 N, the COF reached its minimum at 1000 rpm (0.208) and its maximum at 1500 rpm (0.430). A plausible interpretation is that a lead-rich or mechanically mixed layer lowers the interfacial shear strength at the intermediate speed and is subsequently disrupted by intensified frictional heating and debris generation at the highest speed [5,6]. The EDS point spectra in Fig. 6 test only whether lead-rich patches are present; they do not verify the proposed mechanism.

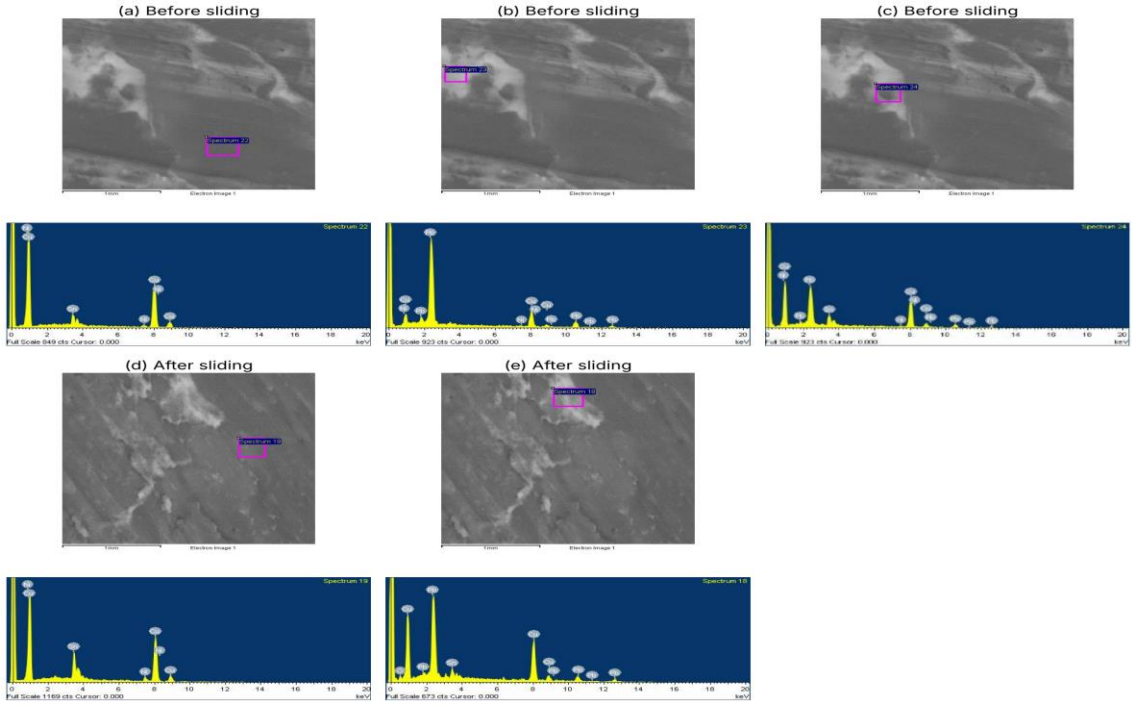

Fig. 6. Scanning electron micrographs (backscattered-electron contrast, 20 kV, ×10,000, scale bar 1 μm) of sample D with EDS point spectra from the marked areas: (a–c) before sliding, Spectra 22, 23 and 24; (d, e) after a sliding wear test, Spectra 19 and 18.

Figure 6 shows electron micrographs of sample D before and after sliding, together with EDS point spectra from the marked areas. Before sliding (Fig. 6a–c), the surface consists of smooth, elongated features with bright and dark areas of different contrast. After sliding (Fig. 6d, e), the surface carries grooves along one direction and bright, irregular patches of smeared Pb-rich material. In backscattered contrast, bright areas indicate a higher mean atomic number, and the spectra agree with this: Spectra 23, 24 and 18 show a strong Pb peak at about 2.3 keV together with Cu, Ni and Sn, whereas Spectra 22 and 19, taken on the darker matrix, show mainly Cu, Ni and Sn. This supports the presence of the lead-rich layer proposed above. The spectra are qualitative point analyses, and a single field cannot show the wear mechanism of the whole surface.

3.6. COF model for sample D

The COF data were fitted by least squares with a linear model that includes a load × speed product:

$$\mu = 0.26336 - 0.003475\mathrm{L} + 2.9667 \times 10^{-5}\mathrm{N} + 3.600 \times 10^{-6}\mathrm{LN} \quad (3)$$

where μ is the COF. The fit gives R^2 = 0.735, RMSE = 0.0367, MAE = 0.0262 and MAPE = 10.1% (Table 3 and Fig. 7). The largest error occurs at 50 N and 1000 rpm, where the model predicts 0.299 against a measured 0.208.

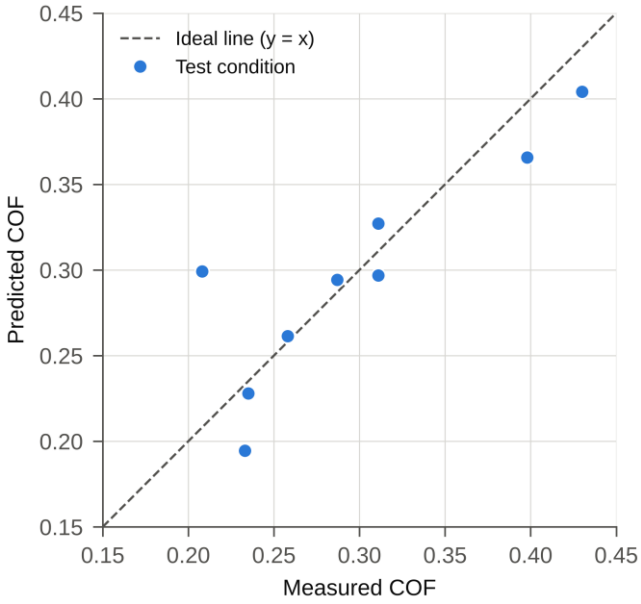

Fig. 7. Measured and predicted COF for sample D, Eq. (3).

The fit is weaker than that for mass loss, as expected, because friction depends on the evolving state of the sliding surface, which load and speed alone cannot capture. Equation (3) should therefore be regarded as a working correlation for the tested range; like Eq. (2), it has four constants for nine points and has not been validated on independent data.

3.7. Generalised models across LTB compositions

Strikingly, wear and friction rank the alloys differently (Table 1). In the screening test, sample B showed the lowest mass loss (0.027 g) but the highest COF (0.560), whereas sample G displayed the lowest COF (0.175) but the highest mass loss (0.690 g); samples D and E occupied an intermediate position for both. Nor did mass loss follow hardness: it was 0.341 g at 57 BHN, 0.027 g at 85 BHN and 0.690 g at 112 BHN. Hardness alone is therefore an unreliable criterion for selecting an LTB grade for wear resistance.

Table 4 presents the results for the five alloys tested at up to three load–speed conditions. Because load and speed were increased simultaneously in these tests, their individual effects cannot be separated for samples B, E, F and G. For sample G, mass loss rose sharply from 0.047 g at 10 N and 500 rpm to 0.690 g at 50 N and 1500 rpm. This behaviour may signal a transition to severe wear in the hardest, tin-rich alloy, which warrants confirmation by worn-surface analysis.

Table 4. Results for five LTB alloys at up to three test conditions, with the predictions of the generalised models.

Sample	Hardness (BHN)	Load (N)	Speed (rpm)	Mass loss, measured (g)	Mass loss, Eqs. (4)–(5) (g)	COF, measured	COF, Eq. (6)
G	112	10	500	0.047	0.008	0.143	0.142
G	112	50	1500	0.690	0.680	0.175	0.220
F	78	10	500	0.008	0.002	0.519	0.417
F	78	50	1500	0.110	0.231	0.468	0.441
B	85	10	500	0.007	0.001	0.483	0.391
B	85	30	1000	0.026	0.050	0.289	0.296
B	85	50	1500	0.027	0.085	0.560	0.426
E	82	10	500	0.006	0.002	0.329	0.407
E	82	30	1000	0.106	0.083	0.256	0.309
E	82	50	1500	0.260	0.261	0.343	0.437
D	88	10	500	0.026	0.005	0.258	0.371
D	88	30	1000	0.130	0.090	0.311	0.278
D	88	50	1500	0.265	0.269	0.430	0.411

To extend the prediction beyond sample D, mass loss was related to load, speed, COF and hardness:

$$\Delta m = 0.04678 \left(\frac{L}{30}\right)^{1.8744} \left(\frac{N}{1000}\right)^{1.6359} \left(\frac{\mu}{0.3}\right)^{-1.6206} \exp(-2.1242h + 0.04317h^2 + 1.2078h^3) \times (t/10) \qquad (4)$$

where t is the test duration in min (t = 10 for all data in Table 4), h = (H − 85)/20 and H is the Brinell hardness. For hardness close to 88 BHN, the result of Eq. (4) is multiplied by a correction factor

$$C = \exp\left\{1.0270 \exp\left[-\left(\frac{H-88}{1.011}\right)^2\right]\right\} \qquad (5)$$

which equals 2.79 at 88 BHN and is practically 1 for the other alloys. The hardness terms up to h^3 allow mass loss to rise and fall with hardness, as the data require.

For the 13 results in Table 4, Eqs. (4) and (5) give R2 = 0.95, RMSE = 0.042 g and MAE = 0.027 g (Fig. 8a). The model follows the high-wear results well, for example 0.680 g against 0.690 g for sample G and 0.269 g against 0.265 g for sample D, but it performs poorly at low wear. For the 6 results below 0.03 g, the predictions are often wrong by a factor of several. These cases raise the MAPE for all 13 results to 66%, whereas the MAPE for the 7 results above 0.03 g is 36%.

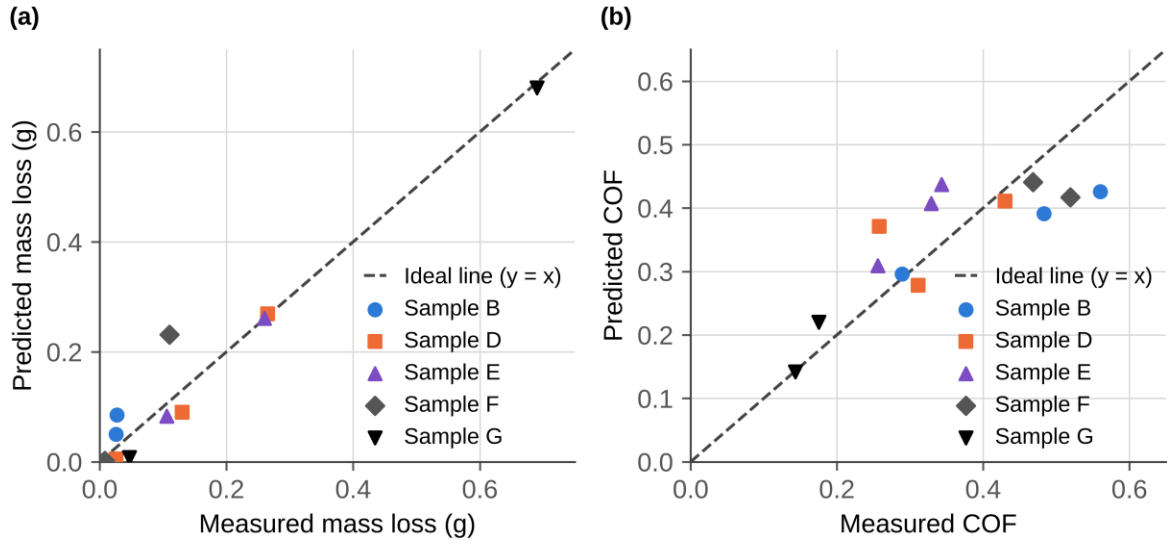

Fig. 8. Measured and predicted values for the generalised models (13 results of Table 4): (a) mass loss, Eqs. (4) and (5); (b) COF, Eq. (6).

Three further limitations must be noted. The model has eight fitted constants for 13 results. The factor C applies to one alloy only and has no physical meaning; it is retained solely so that the equation matches sample D. In addition, the COF is an input to Eq. (4); it is measured in the same test, but it can be estimated from load, speed and hardness with Eq. (6), at the cost of adding the error of Eq. (6) to the prediction.

The COF was related to load, speed and hardness by

$$\mu = 0.561 - 0.385L_n - 0.149N_n - 0.125h - 0.111h^2 + 0.046h^3 + 0.060L_nN_n + 0.030L_nh - 0.008N_nh + 0.209L_n^2 \quad (6)$$

where L_n = L/30 and N_n = N/1000. For the 13 results in Table 4, this gives R2 = 0.65, RMSE = 0.074, MAE = 0.061 and MAPE = 17.5% (Fig. 8b). Because the equation has ten constants for 13 results, it is also a description of this data set rather than a validated predictive tool.

Fig. 9 compares measured and predicted mass loss against hardness for six alloys in the screening test. The model reproduces the rise and fall of mass loss with hardness and is close for samples D, E (0.261 g against 0.260 g) and G (0.680 g against 0.690 g). It overestimates the mass loss of samples F (0.231 g against 0.110 g) and B (0.085 g against 0.027 g) and underestimates that of sample A (0.360 g against 0.409 g), which was not part of Table 4.

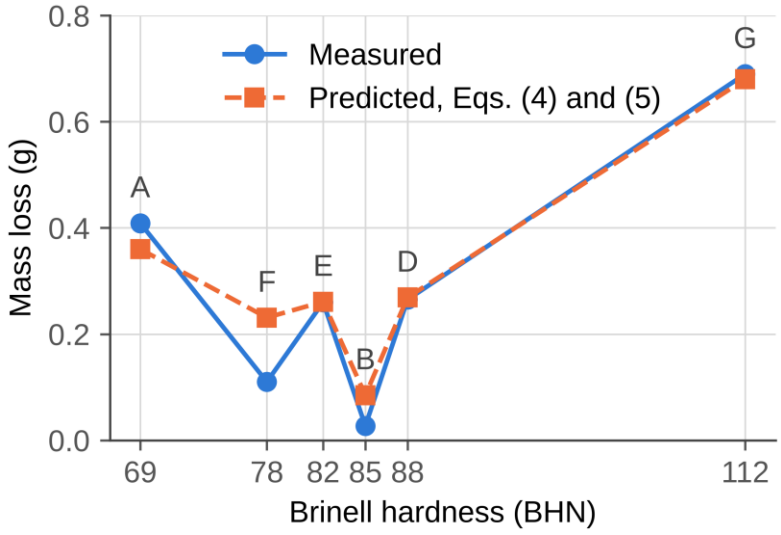

Fig. 9. Measured and predicted mass loss against hardness at 50 N and 1500 rpm for samples A, B, D, E, F and G. Predictions are from Eqs. (4) and (5).

As an additional check, the generalised model was applied to three further alloys, LTB1, LTB4 and LTB5, tested in dry sliding at 20 N and 2000 rpm for 8 min on a 20 mm track. Their compositions (wt%) were Cu–7Sn–3Pb–2Ni–1Zn (LTB2), Cu–7Sn–15Pb–2Ni–1Zn (LTB4) and Cu–10Sn–10Pb–2Ni–1Zn (LTB5, which is sample D). The measured COF values for LTB1, LTB4 and LTB5 were 0.561, 0.518 and 0.499, respectively. Hardness was not measured, so it was estimated from Eq. (1) for LTB1, LTB4 and LTB5, for which, BHN was found as 86, 72 and 83. Because the model was developed for 10 min tests, its predictions were multiplied by 8/10, which assumes a constant wear rate. **The predicted and measured mass losses** were 0.123 and 0.572 g for LTB1 (−78.49%), 0.454 and 0.446 g for LTB4 (+1.79%) and 0.205 and 0.201 g for LTB5 (+1.99%). The model therefore predicted nearer mass loss values for LTB4 and LTB5 while it has not predicted nearer value for LTB1 since LTB1 has the lower weight percentage of Pb than 5% hence, the non applicability of generalized mass loss model for LTB alloy which has the weight percentage of Pb in LTB alloy lower than 5% will be limitation of the model.

3.8. Water-lubricated wear and validation of the dry models

Sample D was tested three times under water lubrication at 50 N and 1500 rpm for 60 min (Section 2.3); the set-up is shown in Fig. 10 and the results are listed in Table 5. Over a sliding distance of 11,310 m, the mass loss was 0.145, 0.155 and 0.118 g (mean 0.139 ± 0.019 g), giving a specific wear rate of (2.46 ± 0.34) × 10^{-7} g/N·m (95% CI ±0.84 × 10^{-7} g/N·m). The COF was 0.174, 0.178 and 0.180 (mean 0.177 ± 0.003; 95% CI ±0.008). Relative to dry sliding at the same load and speed (specific wear rate (2.816 ± 0.049) × 10^{-6} g/N·m, COF 0.430 ± 0.030; Table 5), water lubrication reduced the specific wear rate by 91% and the COF by 59%. Such reductions are commonly attributed to cooling of the contact, partial separation of the surfaces by the water film and flushing of wear debris, although these mechanisms were not verified by surface analysis here.

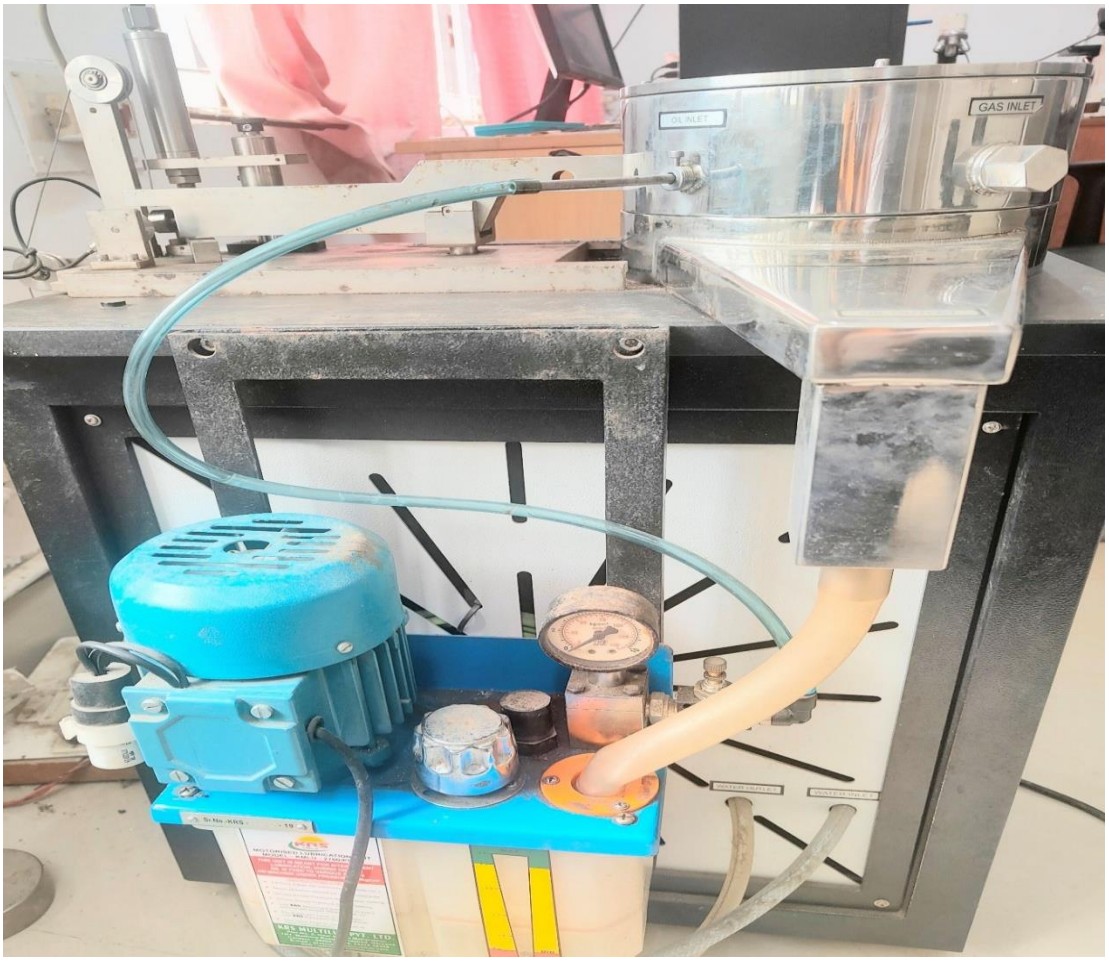

Fig. 10. Pin-on-disc tribometer with the water-lubrication unit used for the water-lubricated wear tests of sample D (50 N, 1500 rpm, 60 min, domestic water).

Table 5. Water-lubricated and dry wear results for sample D (Cu–10Sn–10Pb–2Ni–1Zn, 88 BHN) against EN31 steel at 50 N and 1500 rpm; **track radius 20 mm.**

Test	Duration (min)	Sliding distance (m)	Mass loss (g)	Specific wear rate (10^{-6} g/N·m)	COF
Water 1	60	11,310	0.145	0.256	0.174
Water 2	60	11,310	0.155	0.274	0.178
Water 3	60	11,310	0.118	0.209	0.180
Water, mean ± SD	60	11,310	0.139 ± 0.019	0.246 ± 0.034	0.177 ± 0.003
Dry, mean ± SD (n = 3; COF n = 4)	10	1885	0.265 ± 0.005	2.816 ± 0.049	0.430 ± 0.030

Because the water-lubricated results were not used in any fit, they provide a genuinely independent check of the dry models (Table 6). As the water tests lasted 60 min, the comparison is made on the specific wear rate, which removes the effect of sliding distance. At 50 N and 1500 rpm, Eq. (2) predicts a mass loss of 0.255 g over 1885 m, equivalent to a specific wear rate of 2.70×10^{-6} g/N·m, against the measured $(2.46 \pm 0.34) \times 10^{-7}$ g/N·m; the dry model therefore overpredicts the water-lubricated wear rate about elevenfold (+996%). Eq. (3) predicts a COF of 0.404 against 0.177 (+128%), and Eq. (6) predicts 0.411 (+132%). When the measured water-lubricated COF is entered in Eq. (4), the predicted specific wear rate rises to 1.20×10^{-5} g/N·m, about 49 times the measured value, because Eq. (4) associates a lower COF with higher wear under dry sliding. The dry models therefore cannot be transferred to a water-lubricated contact without correction. A water-lubrication factor λ, defined as the measured water-lubricated value divided by the dry-model prediction, is 0.091 for the specific wear rate (Eq. (2)), 2.05×10^{-2} for the specific wear rate (Eq. (4)) and 0.44 for the

COF (Eq. (3)). Because λ is derived from a single load–speed condition, it constitutes a calibration rather than a validation and should be verified at other loads and speeds.

Table 6. Validation of the dry models against the water-lubricated results of sample D at 50 N and 1500 rpm. No correction factor is applied. Mass-loss predictions for a 10 min test are converted to specific wear rate with s = 1885 m.

Quantity	Dry model	Measured (water)	Predicted	Error	Error (%)
SWR (10^{-6} g/N·m)	Eq. (2)	0.246 ± 0.034	2.70	+2.45	+996
COF	Eq. (3)	0.177 ± 0.003	0.404	+0.227	+128
COF	Eq. (6)	0.177 ± 0.003	0.411	+0.234	+132
SWR (10^{-6} g/N·m)	Eqs. (4)–(5), μ = 0.177	0.246 ± 0.034	12.0	+11.8	+4774

3.9. Bush-life estimate for sample D

This section shows how the water-lubricated wear rate can be used to make a first estimate of bush life in a submersible pump. A 12.5 hp WPIL submersible pump set with a discharge of 1 cusec running at 2950 rpm is taken as an example. The impeller (SS410) has a mass of 2.65 kg and an outer diameter of 164 mm and is assumed to be balanced to grade G6.3 of ISO 21940-11.

The permissible residual unbalance is

$$U = \frac{9549\, G\, m}{n_p} \tag{7}$$

where U is in g·mm, G is the balance grade (mm/s), m is the mass of the rotating part (kg) and np is the pump speed (rpm). This gives U = 54.04 g·mm, equivalent to a residual unbalance mass of about 0.65 g at the impeller radius of 82 mm. The radial force caused by the unbalance is

$$F = U\,\omega^2 \tag{8}$$

where ω is the angular speed (308.9 rad/s) and U is expressed in kg·m. For a residual unbalance of 0.2 g (well balanced) and 0.65 g (permissible limit) at the impeller radius of 82 mm, the force is 1.56 N and 5.08 N, respectively. When the pump operates at its duty point, the hydraulic radial forces on the impeller are balanced and cancel; transient hydraulic loads that arise away from the duty point were not considered. The unbalance force was therefore taken as the bush load and assumed to be shared equally by the two bushes, giving 0.78 N and 2.54 N per bush. A further case of 0.1 g (0.39 N per bush) is also considered.

If a bush of bore diameter d and length b wears uniformly until its diametral clearance has increased by Δc, the mass removed is πd b (Δc/2) ρ, where ρ is the density of the alloy. Equating this to the wear mass K_w W v t gives the life in hours:

$$T = \frac{\pi\, d\, b\, \Delta c\, \rho}{7200\, K_w\, W\, v} \tag{9}$$

where Kw is the specific wear rate in service (g/N·m), W is the load on the bush (N) and v is the sliding velocity (m/s). For a 31.75 mm shaft sleeve at 2950 rpm, v = 4.90 m/s. The bush bore is d = 31.81 mm when new and 32.11 mm when worn out, so the diametral clearance increases by Δc = 0.30 mm (a radial wear of 0.15 mm). The bush length is b = 50.8 mm (2 in). The density of the alloy, ρ = 8.73 g/cm^3, is the mean of three measurements by mass and volume (9.126, 8.673 and 8.406 g/cm^3).

The wear rate in service is the main input. The dry specific wear rate of sample D at 50 N and 1500 rpm is (2.816 ± 0.049) × 10^{-6} g/N·m. Because pump bushes run in water, the water-lubricated value from Section 3.8, K_w = (2.46 ± 0.34) × 10^{-7} g/N·m, is used here.

With this value, Eq. (9) gives an estimated life of about 603 h at 2.54 N per bush (0.65 g unbalance). Because the life is inversely proportional to load, it increases to about 1964 h at 0.78 N per bush (0.2 g unbalance) and to about 3928 h at 0.39 N per bush (0.1 g unbalance). Allowing for the scatter in Kw (±0.34 × 10^{-7} g/N·m), these values range from about 530 to 700 h, from 1730 to 2280 h and from 3450 to 4560 h, respectively. With the dry wear rate, the life at 2.54 N would be only about 53 h, which underlines the decisive role of water lubrication.

These estimates should be regarded as conservative. The pin test was conducted at a nominal contact pressure of 0.99 MPa, far above the pressure on a bush carrying only a few newtons, and the linear scaling of Eq. (9) from test load to service load is a strong assumption. The results therefore illustrate the methodology and provide a lower bound rather than a precise prediction of service life. Actual bush life further depends on water quality, silt content, shaft surface condition, alignment, temperature, load sharing between the bushes and operation away from the duty point.

3.10. Limitations

The main limitations of this study are as follows. (1) Water-lubricated tests were run only at 50 N and 1500 rpm in domestic water; other loads, speeds and silt contents need to be studied. (2) Because the dry test time was fixed, speed and sliding distance changed together. (3) Worn surfaces were examined only by SEM at one magnification and by EDS point spectra at a few spots (Fig. 6), so the wear mechanisms discussed are possible explanations only. (4) The models have many constants relative to the number of results, and the only independent check is the water-lubricated test,

which the dry models overpredicted, so correction factors were applied (Section 3.8). (5) Wear is reported as mass loss and as a mass-based specific wear rate. (6) Samples B, E, F and G were tested at only three conditions (two were retained for F and G after outlier exclusion), and samples A and C at one. (7) The bush-life estimate scales a pin-test wear rate to a much lower service load and applies to operation at the duty point; transient hydraulic loads were not considered. (8) The alloys contain lead, and lead-free alternatives were not studied. Further work should include dry tests at equal sliding distance, SEM–EDS examination of worn surfaces at several conditions, water-lubricated tests over the full load–speed range, and validation of the models on new data.

4. Conclusions

Seven sand-cast LTB alloys were prepared and evaluated in dry sliding against EN31 steel, and the Cu–10Sn–10Pb–2Ni–1Zn alloy (sample D, 88 BHN) was examined in detail at three loads and three speeds and under water lubrication. The principal conclusions are as follows.

(1) The mass loss of sample D in a 10 min test increased with both load and speed. As the load rose from 10 to 50 N, it increased from 0.026 to 0.102 g at 500 rpm and from 0.051 to 0.265 g at 1500 rpm.

(2) The mass-based specific wear rate remained confined to 2.51×10^{-6}–4.30×10^{-6} g/N·m. Mass loss was therefore approximately proportional to load × sliding distance, and much of the apparent speed effect arose from the longer sliding distance at higher speed.

(3) A power-law model with a load–speed term, Eq. (2), fitted the nine mass-loss results with $R^2 = 0.950$, RMSE = 0.0162 g and MAPE = 10.7%.

(4) The COF of sample D varied between 0.208 and 0.430 and did not change monotonically with load or speed. A linear model with a load × speed product, Eq. (3), gave $R^2 = 0.735$ and MAPE = 10.1%.

(5) Hardness ranged from 57 to 112 BHN across the alloys, yet neither mass loss nor COF followed hardness alone, and no single alloy excelled in both wear and friction.

(6) A generalised mass-loss correlation with load, speed, COF and hardness gave R^2 = 0.95 for 13 results on five alloys (after excluding two outliers); it followed the high-wear results but was unreliable below about 0.03 g. A generalised COF correlation gave R^2 = 0.65. When checked against the water-lubricated tests, these dry correlations failed: Eq. (6) overpredicted the COF by 132%, and Eq. (4) overpredicted the specific wear rate about 49-fold, so a correction factor of 2.05×10^{-2} was needed. A further dry test on three other alloys at 20 N and 2000 rpm gave predictions 40–70% below the measured mass loss, so the model should not be applied outside the tested range.

(7) Under water lubrication at 50 N and 1500 rpm, sample D gave a specific wear rate of $(2.46 \pm 0.34) \times 10^{-7}$ g/N·m and a COF of 0.177 ± 0.003, i.e. 91% less wear and 59% less friction than in dry sliding. The dry mass-loss model, Eq. (2), overpredicted this wear rate about elevenfold, so a water-lubrication factor of about 0.091 is required. Using the water-lubricated wear rate, Eq. (9) gave a conservative bush life of about 603 h at the permissible unbalance (0.65 g) and about 1964–3928 h at 0.2–0.1 g for a 12.5 hp WPIL submersible pump operating at its duty point.

(8) The developed generalized mass loss model for LTB alloy are applicable in its goodness for those LTB alloys which has weight percentage of Pb in the range of 5%-20% in copper matrix.

CRediT authorship contribution statement

Ram Dhani Chauhan: Conceptualization, Methodology, Investigation, Formal analysis, Writing – original draft. **Prem Kumar Bharti:** Supervision, Writing – review & editing.

Declaration of competing interest

The authors declare that they have no known competing financial interests or personal relationships that could have appeared to influence the work reported in this paper.

Funding

This research did not receive any specific grant from funding agencies in the public, commercial, or not-for-profit sectors.

Data availability

The data that support this study are given in the article.

Declaration of generative AI and AI-assisted technologies in the manuscript preparation process

During the preparation of this work the authors used Claude (Anthropic) to improve the language, structure and formatting of the manuscript

and to check the calculations. After using this tool, the authors reviewed and edited the content as needed and take full responsibility for the content of the published article.

Acknowledgements

The authors thank Integral University, Lucknow, for assigning the manuscript communication number IU/R&D/2026-MCN0005232, and the USIC laboratory of Dr. Bhim Rao Ambedkar University, Lucknow, for access to its characterization facilities. The author is also thankful to mechanical engineering department of K.N.I.T Sultanupr, UP for providing Pin-On-Disc Tribometer facility and Sri R.K. Rao, AE and their staffs of Irrigation workshop division ,Kanpur for their foundry shop casting facility. The author is also thankful to Sri Akash Yadav, Senior Assistant, Sajja Mandal-1, Irrigation and Water Resources Department, Lucknow for his kind support in typing and formating. The author would like to express his sincere gratitude to his research guide Dr P.K Bharti , HOD, Mechanical Engineering ,Integral university , Lucknow ,UP, India for their continuous unwavering support in this study

References

Ministry of Jal Shakti, Government of India. Ministry of Jal Shakti releases the 6th census report on minor irrigation (MI) schemes. Press Information Bureau; 2023. https://pib.gov.in/PressReleaseIframePage.aspx?PRID=1952939 [accessed 9 October 2026].

Bureau of Indian Standards. IS 318:1981. Specification for leaded tin bronze ingots and castings (second revision). New Delhi: Bureau of Indian Standards; 1981.

Chauhan RD, Bharti PK. A review of tribological excellence of bronze alloys. Discov Appl Sci 2025;7:283. https://doi.org/10.1007/s42452-025-06610-4

Chauhan RD, Bharti PK. An experimental evaluation of tribological & morphological excellence for LTB alloys. Int J Basic Appl Sci 2025;14(7):637–49. https://doi.org/10.14419/v6rpks59

Prasad BK. Sliding wear behaviour of bronzes under varying material composition, microstructure and test conditions. Wear 2004;257:110–23. https://doi.org/10.1016/j.wear.2003.10.021

Pathak JP, Tiwari SN. On the mechanical and wear properties of copper-lead bearing alloys. Wear 1992;155:37–47. https://doi.org/10.1016/0043-1648(92)90107-J

Deyong L, Tremblay R, Angers R. Microstructural and mechanical properties of rapidly solidified Cu–Ni–Sn alloys. Mater Sci Eng A 1990;124:223–31. https://doi.org/10.1016/0921-5093(90)90152-S

Ilangovan S, Sellamuthu R. Effects of tin on hardness, wear rate and coefficient of friction of cast Cu-Ni-Sn alloys. J Eng Sci Technol 2013;8(1):34–43.

Richardson HW, editor. Handbook of copper compounds and applications. New York: Marcel Dekker; 1997.

Manu K, Jezierski J, Ganesh MRS, Shankar KV, Narayanan SA. Titanium in cast Cu-Sn alloys—a review. Materials 2021;14:4587. https://doi.org/10.3390/ma14164587

Tayyaba Q, Butt AQ, Khan TA, Nazar Z, Rehman A, Wu Y. Mechanical alloying of bronze with aluminum and nickel: Impact on corrosion resistance and hardness. J Alloys Metall Syst 2024;8:100136. https://doi.org/10.1016/j.jalmes.2024.100136

Asirinaidu D, Ramajogi Naidu D. Experimental evaluation in the properties of various tin bronzes. Int J Latest Technol Eng Manag Appl Sci 2015;4(6):61–4.

Sobota J, Rodak K, Nowak M. Microstructure and properties of tin bronzes produced by the SPD method. Arch Metall Mater 2019;64:95–102. https://doi.org/10.24425/amm.2019.126223

Seah KHW, Hemanth J, Sharma SC. Effect of the cooling rate on the dendrite arm spacing and the ultimate tensile strength of cast iron. J Mater Sci 1998;33:23–8. https://doi.org/10.1023/A:1004321007806

Hemanth J. Effect of cooling rate on dendrite arm spacing (DAS), eutectic cell count (ECC) and ultimate tensile strength (UTS) of austempered chilled ductile iron. Mater Des 2000;21:1–8. https://doi.org/10.1016/S0261-3069(99)00052-7

Sugita IKG, Soekrisno R, Miasa IM, Suyitno. The effect of solidification rate on morphology microstructures and mechanical properties of 80%Cu-20%Sn bronze alloys. Mater Sci Res India 2010;7:59–66. https://doi.org/10.13005/msri/070106

Gupta R, Srivastava S, Kumar GVP, Panthi SK. Study of microstructure, mechanical properties and wear rate of high leaded tin bronze after multidirectional forging. Procedia Mater Sci 2014;5:1081–9.

Xing J, Soda H, Yang X, Miura H, Sakai T. Ultra-fine grain development in an AZ31 magnesium alloy during multi-directional forging under decreasing temperature conditions. Mater Trans 2005;46:1646–50. https://doi.org/10.2320/matertrans.46.1646

Zhang SZ, Jiang BH, Ding WJ. Wear of Cu–15Ni–8Sn spinodal alloy. Wear 2008;264:199–203. https://doi.org/10.1016/j.wear.2007.03.003

Singh JB, Cai W, Bellon P. Dry sliding of Cu–15 wt%Ni–8 wt%Sn bronze: Wear behaviour and microstructures. Wear 2007;263:830–41. https://doi.org/10.1016/j.wear.2007.01.061

Gao LL, Cheng XH. Effect of ECAE on microstructure and tribological properties of Cu–10%Al–4%Fe alloy. Tribol Lett 2007;27:221–5. https://doi.org/10.1007/s11249-007-9228-7

Moustafa SF, El-Badry SA, Sanad AM, Kieback B. Friction and wear of copper–graphite composites made with Cu-coated and uncoated graphite powders. Wear 2002;253:699–710. https://doi.org/10.1016/S0043-1648(02)00038-8

Rajkumar K, Aravindan S. Tribological behavior of microwave processed copper–nanographite composites. Tribol Int 2013;57:282–96.

Liu Q, Castillo-Rodríguez M, Galisteo AJ, Guzmán de Villoria R, Torralba JM. Wear behavior of copper–graphite composites processed by field-assisted hot pressing. J Compos Sci 2019;3:29. https://doi.org/10.3390/jcs3010029

Wang Y, Yang Q, Chen J, Zhou J. Graphite and nickel containing tin bronze-steel bimetals as lead free bearing materials. Mater Res 2016;19:770–5. https://doi.org/10.1590/1980-5373-MR-2015-0714

Wang X, Tang B, Wang L, Wang D, Dong W, Li X. Microstructure, microhardness and tribological properties of bronze–steel bimetallic composite produced by vacuum diffusion welding. Materials 2022;15:1588. https://doi.org/10.3390/ma15041588

Chauhan RD, Bharti PK. Microstructural & tribological evaluation of sand cast LTB & graphite modified LTBGr alloys. Results in Materials 2026;31:100991. https://doi.org/10.1016/j.rinma.2026.100991